Changes of hygroscopicity and morphology during ageing of diesel soot

2011 Environ. Res. Lett. 6 034026

(http://iopscience.iop.org/1748-9326/6/3/034026)

Environ. Res. Lett. **6** (2011) 034026 (10pp) doi:10.1088/1748-9326/6/3/034026

Changes of hygroscopicity and morphology during ageing of diesel soot

Torsten Tritscher[1], Zsófia Jurányi[1], Maria Martin[2], Roberto Chirico[1,3], Martin Gysel[1], Maarten F Heringa[1], Peter F DeCarlo[1,4], Berko Sierau[2], André S H Prévôt[1], Ernest Weingartner[1] and Urs Baltensperger[1]

[1] Laboratory of Atmospheric Chemistry, Paul Scherrer Institut, 5232 Villigen PSI, Switzerland
[2] Institute of Atmospheric and Climate Sciences, ETH Zurich, Universitätsstrasse 16, 8092 Zurich, Switzerland
[3] Italian National Agency for New Technologies, Energy and Sustainable Economic Development (ENEA), UTAPRAD-DIM, Via E. Fermi 45, 00044 Frascati, Italy
[4] AAAS Science and Technology Policy Fellow Hosted at the US EPA, Washington, DC 20460, USA

E-mail: Ernest.Weingartner@psi.ch

Received 19 April 2011
Accepted for publication 17 August 2011
Published 5 September 2011
Online at stacks.iop.org/ERL/6/034026

Abstract
Soot particles are an important component of atmospheric aerosol and their interaction with water is important for their climate effects. The hygroscopicity of fresh and photochemically aged soot and secondary organic aerosol (SOA) from diesel passenger car emissions was studied under atmospherically relevant conditions in a smog chamber at sub- and supersaturation of water vapor. Fresh soot particles show no significant hygroscopic growth nor cloud condensation nucleus (CCN) activity. Ageing by condensation of SOA formed by photooxidation of the volatile organic carbon (VOC) emission leads to increased water uptake and CCN activity as well as to a compaction of the initially non-spherical soot particles when exposed to high relative humidity (RH). It is important to consider the latter effect for the interpretation of mobility based measurements. The vehicle with oxidation catalyst (EURO3) emits much fewer VOCs than the vehicle without after-treatment (EURO2). Consequently, more SOA is formed for the latter, resulting in more pronounced effects on particle hygroscopicity and CCN activity. Nevertheless, the aged soot particles did not reach the hygroscopicity of pure SOA particles formed from diesel VOC emissions, which are similarly hygroscopic ($0.06 < \kappa_{\mathrm{H-TDMA}} < 0.12$ and $0.09 < \kappa_{\mathrm{CCN}} < 0.14$) as SOA from other precursor gases investigated in previous studies.

Keywords: CCN, H-TDMA, aerosol, diesel soot, organics, hygroscopicity, ageing

1. Introduction

Soot particles are major constituents of atmospheric aerosol, especially in densely populated regions, as they are emitted by combustion processes. Incomplete combustion results mainly in emissions of black carbon (BC), primary organic aerosols (POA) and volatile organic compounds (VOC) in the gas phase. Diesel soot particles are a complex mixture of solid BC (also termed elemental carbon when thermally measured), organic matter (OM), sulfate, ash and other components (Kittelson 1998). We use the term soot in this study for the particles emitted by diesel vehicles, which include both BC and POA. In the atmosphere, VOCs can form secondary organic aerosol (SOA) during oxidative ageing, e.g. under the influence of light as was shown for diesel emissions (Leskinen *et al* 2007, Robinson *et al* 2007, Chirico *et al* 2010). Aerosols and

among them especially BC are known for their potential to cause adverse health effects including acute, chronic, and carcinogenic exposure related health effects (Koelmans *et al* 2006, Pope and Dockery 2006). Some studies, e.g. Kim *et al* (2004) found evidence of respiratory symptoms associated with traffic related pollution. Laden *et al* (2000) associated a higher mortality with fine particles from mobile and coal combustion sources than with other aerosol types.

Atmospheric aerosols also have an influence on the global climate via the direct aerosol effect (by scattering and absorption of visible light) and via the indirect aerosol effect (by changing cloud properties and characteristics (Lohmann and Feichter 2005)). Their contribution to the total radiative forcing is still poorly quantified (IPCC 2007). The hygroscopicity of the particles, i.e. the particles' ability to take up water, and their ability to form cloud droplets are central parameters for the quantification of these effects. BC is a highly light absorbing species and has predominately a warming effect, its quantity depending on the mixing state with light scattering material (Jacobson 2001, Chung and Seinfeld 2002). BC represents (after CO_2) one of the strongest contributions to the current global warming with important consequences for the hydrological cycle, too (Ramanathan and Carmichael 2008). Regionally, impacts of BC can be even larger than those of anthropogenic CO_2. Under ambient conditions, BC, which is in its pure form not hygroscopic, becomes hygroscopic during ageing by, for example, condensation of hygroscopic sulfates or organics (Chung and Seinfeld 2002, Wang *et al* 2010).

The water uptake of soot particles has been investigated in a variety of laboratory and field studies (e.g. Weingartner *et al* 1995, 1997, Baltensperger *et al* 2002, Gysel *et al* 2003, Hitzenberger *et al* 2003, Popovicheva *et al* 2008b, Koehler *et al* 2009, Stratmann *et al* 2010, Rose *et al* 2011). The effect of sulfuric acid and organic coatings has been studied, e.g. by Saathoff *et al* (2003), Zhang *et al* (2008), Xue *et al* (2009), as a proxy for atmospheric ageing. Fractal soot aggregates may collapse under the influence of water and form less fractal, more compact particles, which is referred to as restructuring. Increased restructuring at higher relative humidity (RH) was reported for soot particles from a spark-ignition power generator at high RH (RH = 90–95%) (Weingartner *et al* 1995). Restructuring mechanisms might be capillary condensation, filling of cavities with water or other processes leading to a compaction. Zhang *et al* (2008) also found indications for restructuring at elevated RH for H_2SO_4-coated flame soot, and Gysel *et al* (2003) saw evidence that jet engine combustor soot shows some restructuring if enough sulfate is available. Some studies (Weingartner *et al* 1997, Popovicheva *et al* 2008a, Koehler *et al* 2009) showed restructuring depending on the soot type. However, if restructuring takes place, it is assumed to be an irreversible mechanism that increases the fractal dimension.

Restructuring changes the mechanical mobility of particles and thus influences all mobility based ambient and laboratory measurements. This needs to be taken into account when interpreting hygroscopicity measurements of atmospheric aerosols near sources such as those reported in, for example, Meier *et al* (2009) and Rose *et al* (2011). Restructuring of soot at high RH might have also a direct atmospheric implication by reducing the light absorption as shown by Lewis *et al* (2009).

Here we present a comprehensive study on water uptake, cloud condensation nucleus (CCN) activity and deduced properties of soot nanoparticles from commonly used diesel vehicles. The experiments include freshly emitted diesel soot and a simulation of photochemical ageing processes by condensation of SOA formed from the diesel engine's own VOC emissions under atmospherically relevant conditions. The photochemical ageing processes include among others SOA condensation, oxidation in the gas and particle phase, transformation processes or structural changes which will alter the aerosol properties. The broad aim of this study is to contribute to the understanding of the hygroscopic properties of fresh and aged diesel emissions. Two related studies report additional information on the diesel emission chemical composition and single particle morphology of the diesel emissions observed during the same experiments (Chirico *et al* 2010, Zelenay *et al* 2011).

2. Methods

2.1. Smog chamber setup

Ageing experiments of diesel soot were conducted in the smog chamber at the Paul Scherrer Institute (PSI). The 27 m^3 smog chamber with xenon lamps for simulation of sunlight induced photochemical ageing is described elsewhere (Paulsen *et al* 2005). We performed experiments with exhaust from two commonly used diesel vehicles: a EURO3 Opel Astra 2.0 DTI from February 2002 with a diesel oxidation catalyst (DOC) but no particle filter and a EURO2 Volkswagen Transporter TDI Syncro from December 2000 with no emission after-treatment.

The gaseous and particulate emissions from the tailpipe of the vehicle were injected via a heated (150 °C) inlet system including a heated ejector dilution unit (first dilution step, dilution ratio ~1:7) into the chamber, see table 1 for an overview of the experiments. The final dilution factor in the initial clean and humidified (~50% RH) smog chamber was determined by CO_2 concentration measurements and ranged from 60 to 120 (225–875 for the pure gas phase experiments, see section 2.2). The residence time of the emissions in the inlet system was <10 s. The individual dilution factors and further details such as temperature and gas phase concentration of each experiment can be found in table 1 in Chirico *et al* (2010). The inlet system serves mainly as an extended car tailpipe, while the smog chamber corresponds to the diluted and cold conditions in the atmosphere, where volatile substances may condense.

In some experiments a heated (150 °C) particle filter in the inlet system was used to inject only the gas phase compounds of the diesel exhaust into the smog chamber. We refer to those experiments as pure gas phase experiments. Chirico *et al* (2010) provide further technical details on the smog chamber setup and the performed diesel emission experiments, and their experiments' numbers are adopted here (table 1).

Table 1. Smog chamber experiment overview with experiment number (exp. no.) adopted from Chirico *et al* (2010) and experiment date. The mass concentrations of BC, POA, and OA (=SOA + 'aged' POA after 5 h ageing) are presented for each experiment.

Exp. No.	Date (dd.mm.yyyy)	BC (μg m^{-3})	POA (μg m^{-3})	OA (5 h) (μg m^{-3})	Comments
EURO3, Opel Astra, with DOC; idle conditions					
8	17.08.2009	18.5	3.46	3.91	Warm idle
9	19.08.2009	22.3	3.76	4.82	Single particle analysis[a]
10	21.08.2009	25.3	11.3	12.6	
11	26.08.2009	22.2	5.4	7.34	
12	24.08.2009	0	0	4.00	Only gas phase
EURO2, VW Transporter, without after-treatment; idle conditions					
13	31.08.2009	17.6	2.61	8.34	
14	02.09.2009	18.8	3.35	13.9	Single particle analysis[a]
15	04.09.2009	13.5	2.06	15.0	
16	28.09.2009	14.6	3.16	6.70	
17	30.09.2009	13.6	1.76	9.42	
18	02.10.2009	0	0	5.41	Only gas phase

[a] For details on the single particle studies see Zelenay *et al* (2011).

2.2. *Instrumentation*

The PSI smog chamber is equipped with several gas and particle phase instruments, including a scanning mobility particle sizer (SMPS) for measurement of the particle number size distribution from about 20 to 700 nm. The custom-built SMPS includes a long column differential mobility analyzer (DMA, model 3071, TSI) and a condensation particle counter (CPC, model 3022A, TSI) operated with aerosol and closed-loop sheath flow rates of 0.3 and 3 l min^{-1}, respectively. An Aerodyne high-resolution time-of-flight aerosol mass spectrometer (AMS) was used to measure the chemical composition of the non-refractory aerosol components and to determine the atomic O:C ratio of the organic aerosol species with high time resolution. The aerosol light absorption coefficient was determined with a multiangle absorption photometer (MAAP, Thermo model 5012) from which the BC mass concentration was derived using the mass absorption efficiency (MAE) provided by the manufacturer (6.6 m^2 g^{-1} at 630 nm). The MAE of BC can change by coating with organic material. However, the ratio of BC measured by MAAP and a single particle soot photometer (SP2) showed less than 10% change after 5 h of ageing and therefore we consider the coating effect on the BC measurement by MAAP to be small for our experiments. Details on the BC determination and comparison of the methods are given in Chirico *et al* (2010).

Hygroscopic diameter growth factors (GFs) of particles, defined as the ratio between their mobility diameter D(RH) at high RH and their dry mobility diameter D_0, were measured online by a hygroscopicity tandem differential mobility analyzer (H-TDMA) for particles with dry diameters $D_0 = 35$, 50, 75, 100, 150, 200 and 300 nm. A detailed description of the custom-built H-TDMA is provided in Tritscher *et al* (2011). Briefly, the aerosol is dried to RH $< 15\%$ before a first differential mobility analyzer (DMA1) is used to select a quasi-monodisperse aerosol with D_0. The size selected particles are then humidified to a high RH (95% in this study). After a residence time of 26 s, the resulting size distribution of the humidified particles is determined by a second DMA (DMA2) and a CPC (model 3022A, TSI). Growth factors are obtained using the inversion algorithm from Gysel *et al* (2009). All humidified sections of the H-TDMA are placed in a temperature controlled housing in order to guarantee accurate RH control and measurement.

Experiments were conducted with and without an additional pre-humidifier (RH = 95–100%) in front of the H-TDMA diffusion drier. This additional humidification cycle (residence time < 1 s) aims at collapsing fractal-like particles as much as possible prior to drying and size selection in the H-TDMA. Small sizing offsets between the two DMAs were accounted for by dry measurements at RH $< 10\%$ in DMA2 after each experiment, for which the measured GF must be unity. The accuracy of the H-TDMA measurements was verified with measurements of pure ammonium sulfate particles and the error in GF was typically $<1\%$. The maximum error due to sizing is ± 0.01 in GF while the GF uncertainty due to RH uncertainty depends on the observed hygroscopic growth factors. For small GF (<1.05) the GF uncertainty attributed to RH uncertainty is typically $<\pm 0.01$, and increases for higher GF (to about ± 0.03 for a GF of 1.3 at 95% RH). The GFs measured in the RH range between 93 and 97% were recalculated to 95.0% RH following (Gysel *et al* 2009, their equations (3), and (6)), using a single-parameter growth curve parametrization for correcting small RH differences. The applied corrections were very small as only measurements in a small band of $\pm 2\%$ RH were included. Applying the RH correction minimizes systematic biases when reporting GFs at a constant target RH from measurements acquired across a narrow range of RHs around the target RH.

The particles' critical supersaturation (SS_{crit}) was determined with a commercial continuous-flow stream wise thermal-gradient cloud condensation nuclei counter (CCNC, DMT model CCN-100). A DMA was used to select a dry, quasi-monodisperse aerosol, which was then fed into a CPC and the CCNC for parallel measurements of the total particle number concentration (N_{CN}) and the CCN number concentration (N_{CCN}), respectively. N_{CCN} was measured at 10 or more different supersaturations (SSs) chosen to completely cover the whole activation step. SS_{crit} is defined as the

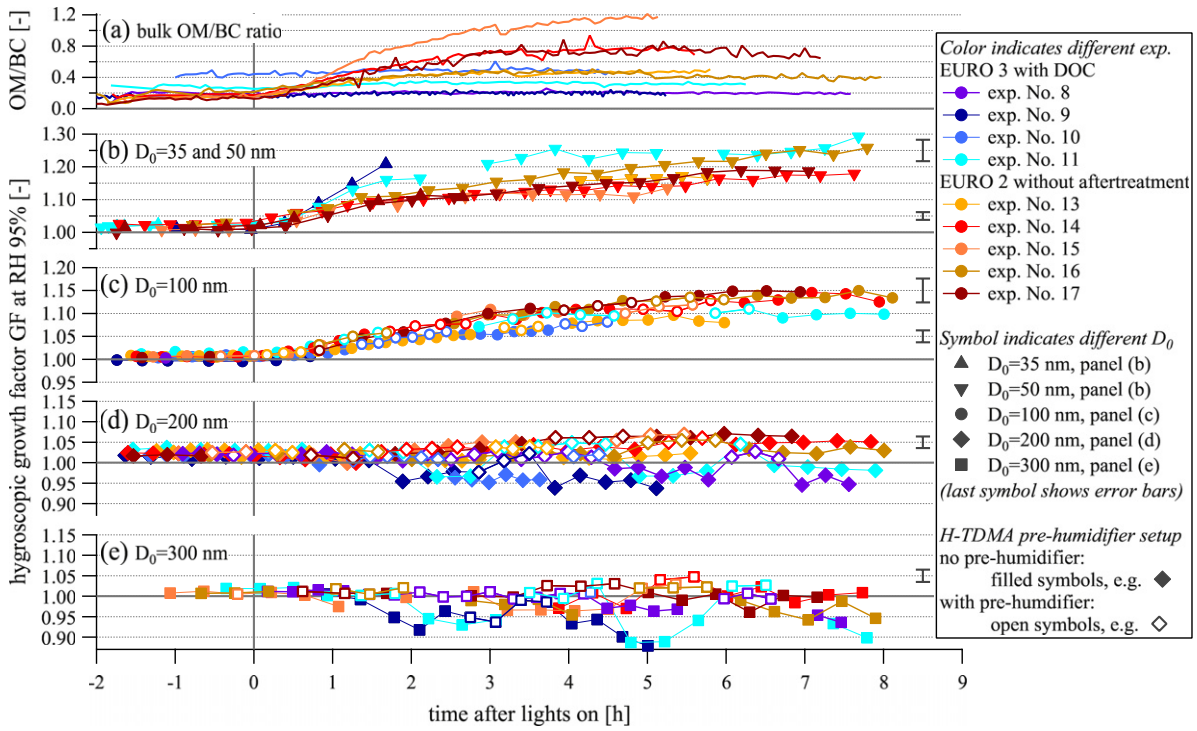

Figure 1. Evolution of diesel particle properties during photochemical ageing. Panel (a) shows the bulk OM/BC ratio, and panels (b)–(e) the hygroscopic growth factor GF at RH = 95% for D_0 = 35/50, 100, 200 and 300 nm, respectively. The individual experiments are distinguished by cold/bluish colors for the EURO3 experiments (diesel car with DOC) and by warm/reddish colors for EURO2 (diesel van without after-treatment system). Open symbols represent periods with a pre-humidifier in front of the H-TDMA instrument and filled symbols periods without a pre-humidifier. Exemplary error bars are shown for each diameter at the right end of the panels (b)–(e).

SS where 50% of the singly charged particles are activated, i.e. N_{CCN}/N_{CN} = 50%. SS_{crit} was determined by fitting two sigmoid functions to the activation steps of singly and doubly charged particles (Jurányi *et al* 2009). The CCNC was calibrated six times during the campaign using pure, size selected ammonium sulfate particles. The theoretical SS_{crit} (D_0) values for ammonium sulfate were obtained from the ADDEM model (Topping *et al* 2005). The relative deviations between the individual calibrations were less than 5% and this can be considered to be the accuracy of the SS for our CCNC measurements. CCNC measurements were performed at D_0 = 50, 75, 100, 150, 200 and 300 nm. At least one D_0 was simultaneously measured by the CCNC and the H-TDMA in order make results directly comparable.

2.3. Hygroscopicity parametrization

The hygroscopicity (both at sub- and supersaturation) was parametrized with the single hygroscopicity parameter κ, which was introduced by Petters and Kreidenweis (2007) assuming a surface tension of pure water. The use of κ allows for direct comparison between H-TDMA and CCNC results and with other studies. κ = 0 corresponds to GF = 1 and represents a spherical, insoluble but wettable particle that would activate at its Kelvin SS_{crit}, also termed the 'Kelvin line' (Koehler *et al* 2009). κ-theory assumes spherical particles with a defined volume equivalent diameter (D_{ve}). In our experiments particles are selected by mobility diameter, which is different from their volume equivalent diameter, as soot particles are non-spherical. Therefore the term 'apparent κ' is used for all soot particles. The effect and consequences of the non-sphericity of the particles will be discussed in more detail later.

3. Results and discussion

Chirico *et al* (2010) showed that the BC and POA emission factors of the investigated EURO3 and EURO2 vehicles were similar, while their POA was chemically somewhat different. In contrast, the SOA production was about ten times smaller for the EURO3 vehicle (0.02 g SOA/kg fuel) compared to the EURO2 (0.25 g SOA/kg fuel), due to the fact that the DOC in the EURO3 vehicle removes a major fraction of the VOCs by oxidation. Consequently one can expect similar physical properties of the fresh emissions from the EURO2 and EURO3 vehicles but different ageing effects. Figure 1(a) shows the evolution of the organic to BC mass ratio (OM/BC) as a function of time after lights on (TALO) for the EURO3 (bluish colors) and the EURO2 (reddish colors). The initial OM/BC ratio is mostly below ~0.35 and similar for both cars and it increases with photochemical ageing (TALO > 0). This effect is much smaller for the EURO3 with distinctly less SOA production. The O:C ratio (not shown) ranged from 0.10 (EURO3) to 0.19 (EURO2) for fresh POA and increased to 0.24–0.37 for the OM (aged POA + SOA) after 5 h of photochemical ageing. It can thus be expected that fresh POA exhibits only a little water uptake at 95% RH, while ageing will

increase the hygroscopicity of the OM (see also discussion of pure gas phase experiments).

In figures 1(b)–(e) the development of hygroscopicity at 95% RH is shown for different dry sizes. Before ageing, the particles with D_0 between 35 and 300 nm show virtually no hygroscopic growth (GF = 1–1.02) in agreement with the fact that the particles are a combination of insoluble BC with non-hygroscopic POA. Particles with $D_0 = 200$ nm are an exception with slightly higher GFs (1.02–1.04). The reason for this is unknown but a calibration bias can most likely be excluded. Popovicheva *et al* (2008a) reported irreversible swelling of BC particles exposed to high RH due to a change of the micropore structure, however, it is unclear why such an effect should specifically influence the 200 nm particles. Hygroscopic growth factors of soot particles increase with photochemical ageing. This is attributed to condensation of SOA, which is moderately hygroscopic (Massoli *et al* 2010, Duplissy *et al* 2011) due to a higher O:C ratio. GF values after ageing are on average higher for the emissions from the EURO2 vehicle compared to the EURO3 vehicle, consistent with the higher SOA formation potential of the former. We can see from the data (OM/BC ratios and GF values in figure 1) that we are able to get reproducible results, in the sense that experiment to experiment variability is smaller than differences between EURO2 and EURO3 experiments. The smallest particles show the highest though still only moderate hygroscopic growth (GF up to 1.25 for $D_0 \leqslant 50$ nm). Less hygroscopic growth is observed at $D_0 = 100$ nm ($1.05 < \mathrm{GF} < 1.15$ at TALO > 5 h) and hardly any hygroscopic growth or even shrinkage (i.e. GF < 1) at $D_0 = 200$ and 300 nm. This size dependence is partially attributed to relatively more efficient mass acquisition by SOA condensation for smaller particles. It is important to note that figure 1(a) represents the bulk chemical composition and reflects the chemical composition dominated by the larger particles.

Furthermore, a restructuring is seen, predominately for EURO3 emissions with low to medium initial OM/BC ratios and for particles with $D_0 = 200$ and 300 nm (diamond and square bluish filled symbols in figures 1(d) and (e)). At least 1 h ageing time in the smog chamber or longer is needed before larger particles show detectable restructuring (GF < 1) at RH of 95%. No restructuring could be detected for the fresh diesel soot. This is most probably due to the fact that the fresh particles are not sufficiently hygroscopic to take up enough water required to induce restructuring. The magnitude of the observed restructuring varies and reaches GF changes up to −10% but generally tends to increase with particle size and partially with time. The difference between the filled and open symbols in figures 1(d) and (e) indicates that most restructuring occurs in the pre-humidifier, when it is added in front of the H-TDMA. Addition of the pre-humidifier thus leads to a higher measured GF as the restructuring is irreversible. The observed restructuring demonstrates that the investigated combustion particles are often not spherical and that condensation of water (or SOA) can make them more compact. The mobility diameter (D) of a non-spherical particle is generally larger than the geometric diameter of a spherical particle with equal volume (DeCarlo *et al* 2004) and thus the measured GF provides a lower limit for the true hygroscopic growth due to water uptake. The same applies to the resulting κ values. Therefore we call them 'apparent κ', representing the mobility based measurements, which might be smaller than the volume equivalent water uptake due to restructuring and morphology changes of the non-spherical particles.

An example of the evolution of the CCN properties along with corresponding GF measurements is shown in figure 2 for a typical experiment with the EURO3 vehicle (here exp. no. 9). Restructuring due to water uptake is again visible for the larger diameters, while the smallest particles with $D_0 = 35$ nm show a rapid increase in GF, indicating particles dominated by OM (figure 2(a)). The CCN activation spectra of $D_0 = 200$ nm particles are presented in figures 2(b)–(e) for different ageing times. Freshly emitted soot particles (TALO $\leqslant$ 0) are completely CCN inactive up to the maximum possible instrumental SS of 1.35%, which is well above its Kelvin $\mathrm{SS_{crit}}$ (1.01% is the SS at which non-hygroscopic but wettable 200 nm spherical particles would activate). This CCN inactivity might be interpreted as hydrophobic particles, probably erroneously as addressed in more detail below.

Figure 2 also shows that photochemical ageing has a strong effect on measured CCN activation. About 50% of the particles show CCN activation at TALO = 0.70–1.13 h (figure 2(d)) and all particles are CCN active with an apparent κ value of ∼0.008 at TALO = 2.70–3.12 h (figure 2(e)). The plateau at 50% in the SS scan of figure 2(d) indicates that not all particles are activated at the highest SS, which might be attributed to externally mixed particles with distinctly different properties, e.g. shape or hygroscopicity. In contrast to the H-TDMA measurements, a pre-humidifier was not applied in front of the DMA which selected the particles for the CCN measurements. Thus the increased CCN activity in figures 2(c)–(e) is not caused by a compaction in the pre-humidifier. Instead it is the result of ageing processes, which includes among others SOA condensation. This can lead to a higher effective density of the soot particles and thus a larger volume equivalent diameter when selecting at constant mobility diameter. Also, the SOA condensation itself will cause an increase in the hygroscopicity of the particles.

It is possible that a threshold OM/BC ratio or a threshold oxidation of the surface is needed for collapsing the particles. The transition from CCN inactive (AF = 0 at SS = 1.35%) to completely CCN active particles (AF = 1 at SS = 1.35%) at $D_0 = 200$ and 300 nm occurred within about 1 h after lights on in experiment no. 11 with the EURO3 car (not shown). This timescale compares to ambient measurements in Mexico City which suggested that a few hours of ageing were sufficient to increase the hygroscopicity of mixed POA/BC particles; which is a significantly shorter timescale than assumed in many global models (Wang *et al* 2010).

Fresh diesel exhaust particles are known to be of non-spherical fractal-like shape (see e.g. Park *et al* 2003, and references therein). Consequently the volume equivalent diameter (D_{ve}) of a soot particle is expected to be smaller than its mobility diameter (D). From a theoretical point of view D_{ve} is more appropriate for CCN activation than the mobility diameter D. Shape effects are thus a possible reason

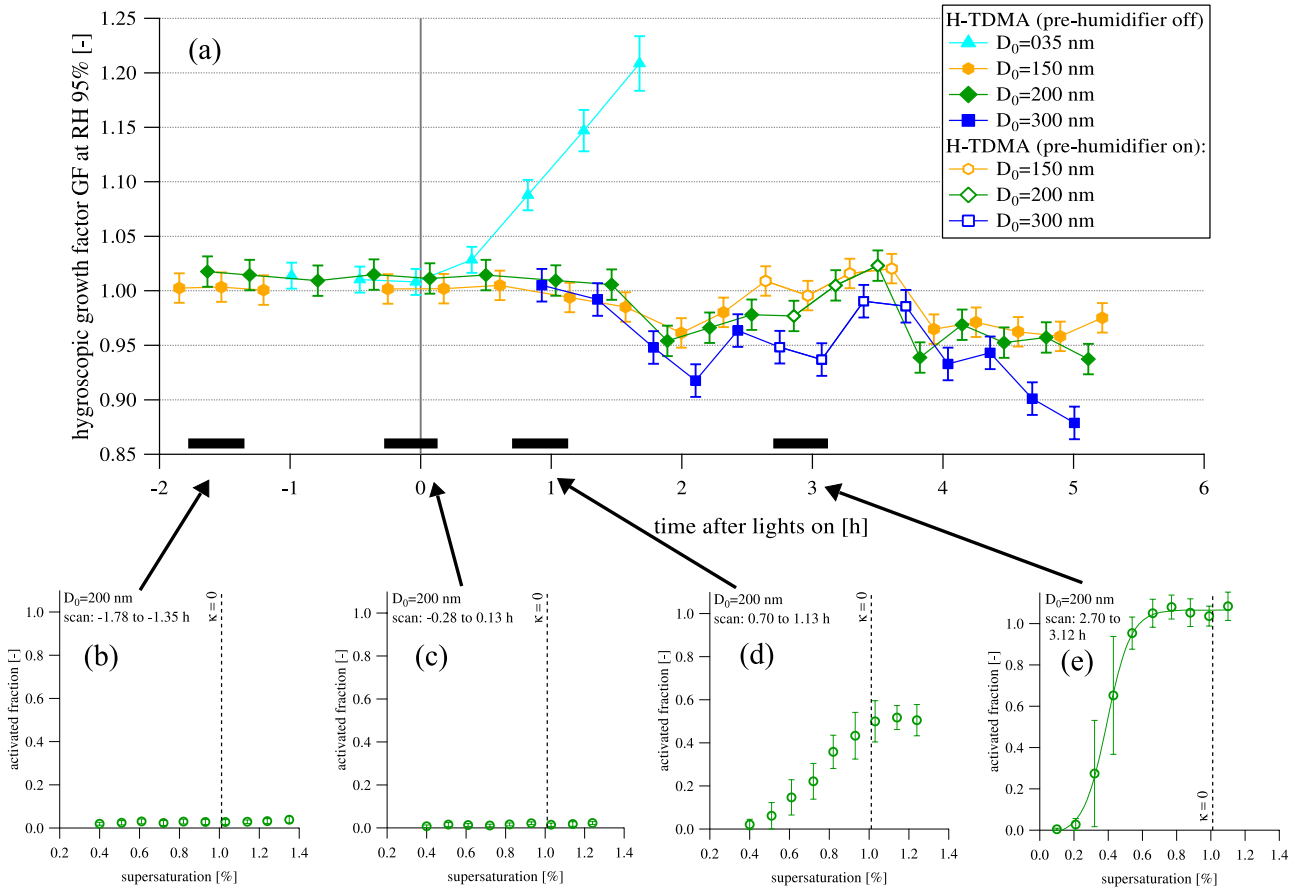

Figure 2. (a) Temporal evolution of the hygroscopic growth factor GF at RH 95% for different dry mobility diameters D_0 during the EURO3 experiment no. 9 with error bars representing the uncertainty in GF. Open symbols indicate periods when the pre-humidifier in front of the H-TDMA was on. (b)–(e) CCN activation spectra for $D_0 = 200$ nm during experiment no. 9. The vertical dashed lines represent $\kappa = 0$ for 200 nm spherical particles; black bars and arrows denote the experimental times of the CCN scans, and error bars represent one standard deviation of the activated fraction.

Table 2. The effective density (ρ_{eff}) and corresponding dry volume equivalent diameter (D_{ve}) of fresh diesel soot emission particles with dry mobility diameter (D_0) of 200 and 300 nm assuming a bulk density (ρ_{bulk}) of 2.0 g cm^{-3}. The critical κ value (κ_{crit}) at SS = 1.35% is calculated from Köhler theory assuming ρ_{eff} values from Park *et al* (2003). (Note: $D_{\text{crit}} = 153.8$ nm at SS = 1.35% and $T = 29\,^{\circ}$C in the CCNC.)

D_0 (nm)	ρ_{eff} (g cm^{-3})	$\rho_{\text{eff}}/\rho_{\text{bulk}}$ (—)	$D_{\text{ve}} = D_0(\rho_{\text{eff}}/\rho_{\text{bulk}})^{1/3}$ (nm)	κ_{crit} at SS = 1.35% (—)
200	0.10	0.05	74	0.013
200	0.70	0.35	141	0.000084
200	0.91	0.45	154	0
200	>0.91	>0.45	>154	Hydrophobic
300	0.10	0.05	111	0.0016
300	0.27	0.14	154	0
300	>0.27	>0.14	>154	Hydrophobic

for the complete absence of CCN activation at SS above the Kelvin line (apparent $\kappa = 0$). The effective density, $\rho_{\text{eff}} = \rho_{\text{bulk}}(D_{\text{ve}}/D)^3$, of fresh diesel soot particles with diameters between 200 and 300 nm is expected to be in the range of ~0.10–0.70 g cm^{-3} (Park *et al* 2003). ρ_{bulk} is the bulk material density. A soot particle with a dry mobility diameter $D_0 = 200$ nm and ρ_{eff} of 0.10 g cm^{-3} has a D_{ve} of 74 nm (assuming $\rho_{\text{bulk}} = 2.0$ g cm^{-3}) and it will be CCN inactive at SS = 1.35% if its κ value is smaller than 0.013 (see table 2). The critical κ value (κ_{crit}), where particles activate, corresponding to ρ_{eff} of 0.70 g cm^{-3} at $D_0 = 200$ nm is 0.000084. This means that the observed CCN inactivity can solely be explained by non-spherical shape, even if the soot is wettable, as long as its κ is close to zero. All wettable particles with $D_0 = 200$ nm would be CCN active at SS = 1.35% ($\kappa_{\text{crit}} \leqslant 0$) if ρ_{eff} was 0.91 g cm^{-3} or higher, in which case the observed CCN inactivity could only be explained by additional hindering effects such as hydrophobicity of the soot surface.

Similarly for particles with $D_0 = 300$ nm the observed CCN inactivity can be explained by shape effects alone

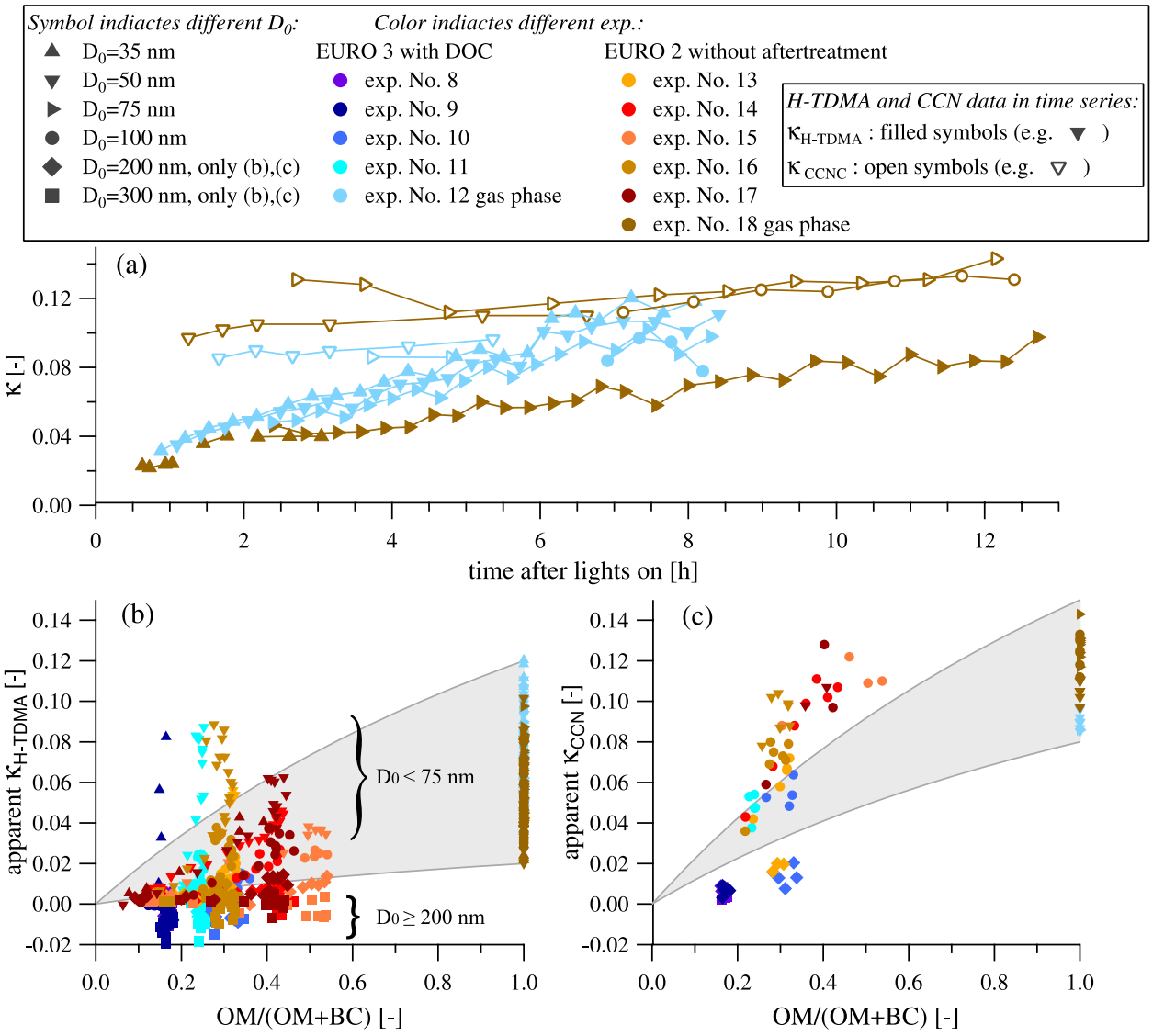

Figure 3. (a) Temporal evolution of κ for two pure gas phase experiments for H-TDMA (filled symbols) and CCNC (open symbols); symbol shape indicates the D_0 of the analyzed particles. The individual experiments are distinguished by cold/bluish colors for the EURO3 experiments (diesel car with DOC) and by warm/reddish colors for EURO2 (diesel van without after-treatment system). (b), (c) The correlation of apparent $\kappa_{\mathrm{H-TDMA}}$ and apparent κ_{CCN} with OM fraction, respectively. The gray shading represents the expected κ range derived from ZSR mixing calculations. It is important to note that (c) only contains data points after the aerosol has become CCN active as apparent κ_{CCN} cannot be determined for CCN inactive aerosol.

according to our calculations in table 2, if ρ_{eff} is lower than 0.27 g cm^{-3}. κ values close to zero are plausible for fresh soot, as the elemental carbon is insoluble ($\kappa = 0$) and the fresh POA is likely to have a κ smaller than ~0.1 due to its low O:C ratio (see above). κ values greater than 0.1 may be found due to fuel impurities such as sulfur (Gysel *et al* 2003). However, in our experiments the sulfate content of the soot is expected to be negligible as low sulfur fuel was used (<50 ppm) and the AMS did not detect particulate sulfate (Chirico *et al* 2010). In summary, the observed absence of CCN activation of the fresh emissions can mainly be explained by shape effects, while further hindering effects such as hydrophobicity cannot completely be excluded.

Zelenay *et al* (2011) used a scanning electron microscope (SEM) to characterize single diesel soot particles from the same experiment (no. 9) as shown in figure 2. They showed that fresh diesel particles had a highly non-spherical shape and that the particles' morphology became more compact with ageing, thereby confirming the above observations. In addition, the water uptake of single soot particles (also for experiment no. 9) was analyzed in a custom built cell with absorption maps from scanning transmission x-ray microspectroscopy (Zelenay *et al* 2011). Even some unprocessed, primary diesel soot particles from the EURO2 took up water, which was not observed for the EURO3. The water uptake for both EURO2 and EURO3 increased upon processing, which is in good agreement with the findings presented and discussed here.

In the following, we compare the hygroscopic growth with the CCN activity (both expressed in terms of κ-values), beginning with the pure gas phase diesel experiments (figure 3(a)), when neither POA nor BC are present. $\kappa_{\mathrm{H-TDMA}}$ values are ~0.02 after nucleation of the SOA (TALO ~ 0.5 h)

for both EURO2 and EURO3 diesel emissions. Ageing results in a continuous increase of $\kappa_{\mathrm{H-TDMA}}$, reflecting the increase of O:C ratio (not shown) in agreement with Duplissy *et al* (2011). $\kappa_{\mathrm{H-TDMA}}$ values as high as ∼0.12 are eventually reached after several hours. Even after 8–12 h of ageing no stable κ is reached and therefore hygroscopicity of the pure diesel SOA may increase further with further ageing time. The pure diesel SOA measurements are not influenced by non-sphericity effects as these particles are spherical. Therefore the obtained κ values are not biased and they can be used, along with the assumption of insoluble BC, for calculating the volume equivalent water uptake of aged non-spherical soot, if the BC and OM volume fraction of the particles is available. It is noteworthy that the $\kappa_{\mathrm{H-TDMA}}$ values reached in the pure gas phase diesel experiments compare well with the apparent $\kappa_{\mathrm{H-TDMA}}$ values reached in normal diesel exhaust experiments at the smallest D_0 (shown as GF in figure 1(a)). This is consistent with small soot particles becoming OM dominated after SOA condensation.

Initial κ_{CCN} values of pure gas phase diesel SOA are 0.08 and larger and thus distinctly higher than initial $\kappa_{\mathrm{H-TDMA}}$ values (see figure 1(a)). The effect of ageing on κ_{CCN} is only small and κ_{CCN} always remains below ∼0.14 even after several hours. A weak influence of the changing O:C ratio on κ_{CCN} is in agreement with the observations by Jurányi *et al* (2009) and Massoli *et al* (2010) for different SOA precursors while the influence of the O:C ratio under subsaturated conditions seems to be higher (Duplissy *et al* 2011). First we can exclude artifacts from shape effects as pure diesel SOA particles are spherical. Petters *et al* (2009) brought up theoretical arguments that the O:C ratio of SOA has much less influence on CCN activation than on hygroscopic GFs as non-ideal interactions lose out in importance with water activity approaching unity, i.e. κ can be expected to be solution concentration dependent. Other effects such as surface tension reduction or limited solubility may also play a role.

Figures 3(b) and (c) show the correlation of apparent $\kappa_{\mathrm{H-TDMA}}$ and apparent κ_{CCN} with the organic mass fraction (OM/(OM + BC)). The data points at unit organic mass fraction are from the pure gas phase experiments. The spread in apparent κ at unit organic mass fraction originates mainly from the ageing process (see figure 3(a) for the temporal evolution of exactly the same pure gas phase experiments). The gray shadings reflect κ values calculated with the Zdanovskii–Stokes–Robinson (ZSR) mixing rule (Petters and Kreidenweis 2007) for mixtures of BC ($\kappa = 0$) with OM (range of κ values taken from the gas phase experiments) and assuming densities of $\rho_{\mathrm{OM}} = 1.27\ \mathrm{g\,cm^{-3}}$ and $\rho_{\mathrm{BC}} = 2\ \mathrm{g\,cm^{-3}}$ (Cross *et al* 2007, Park *et al* 2003). The apparent $\kappa_{\mathrm{H-TDMA}}$ in figure 3(b) range from −0.02 to 0.09 reflecting the main results already discussed with figure 1: first, the emissions of the EURO2 vehicle (reddish symbols) typically reach higher organic mass fractions and thus also higher growth factors than the emission of the EURO3 vehicle (bluish symbols). Second, the smaller particles are more hygroscopic than larger particles due to a relatively higher organic mass fraction and less influence from restructuring. Third, ageing results in an increase of the organic mass fraction and hygroscopicity which could already be seen in figure 1, and which is also reflected in an increase in apparent $\kappa_{\mathrm{H-TDMA}}$ as seen, for example, for exp. no. 14 in figure 3(b) (in combination with figure 1). The same trends regarding the influence of engine type, particle size, and ageing are also observed for κ_{CCN} values, though for equal experiments κ_{CCN} values are typically higher than $\kappa_{\mathrm{H-TDMA}}$ values, which has mainly two reasons. First of all it has to be emphasized that figure 3(c) only contains data points after the aerosol has become CCN active, as κ_{CCN} cannot be determined for CCN inactive aerosol. Second, the κ value of the OM is higher at supersaturated conditions compared to RH = 95%, as previously shown with figure 3(a). The fact that data points from larger and smaller particles fall below and above the theoretically expected range derived from ZSR calculations (gray shading in figures 3(b) and (c)) can be explained by the following two effects: first, apparent κ values are biased in a vertical direction toward lower values if non-spherical particles are selected by a DMA and if restructuring occurs. Second, the horizontal axis represents OM mass fractions of the bulk aerosol. Any size dependence of the OM mass fraction, which can be expected for OM acquisition by condensation, results in horizontal biases. Nevertheless the bulk OM mass fraction is still a useful indicator as changes of the OM mass fraction at any size cut will be correlated with changes of the bulk composition.

4. Conclusions

The hygroscopicity of fresh and photochemically aged soot from two commonly used diesel vehicles has been studied under atmospherically relevant conditions with two independent online methods below and above water vapor saturation. Fresh diesel soot particles show no hygroscopicity and little or no interaction with water. The main reason for the absence of activation even at a supersaturation where an insoluble but hydrophilic particle should be activated is the uncertainty introduced by selecting non-spherical particles. However, we cannot exclude the possibility that fresh diesel soot is hydrophobic. The hygroscopicity of photochemically aged soot shows ranges of the apparent κ of −0.02 to +0.09 for $\kappa_{\mathrm{H-TDMA}}$ and 0–0.13 for κ_{CCN}. Aged diesel soot from a vehicle without any after-treatment (EURO2) shows higher hygroscopicity and higher OM/BC fractions than aged particles from a vehicle with DOC (EURO3). During the ageing processes more SOA was formed in the EURO2 experiments, while the SOA potential in the EURO3 experiments was reduced by the DOC due to lower VOC concentrations in the gas phase. The hygroscopicity is directly linked to the SOA amount formed from the diesel gas phase emissions. This is also seen for both vehicles (EURO2 and EURO3) in the size-dependent hygroscopicity, which is higher for smaller particles which have a higher fraction of SOA coating and thus a higher OM/BC fraction than the larger particles.

The mobility diameter based detection of CCN activation behavior and water uptake of fresh and aged diesel soot is strongly affected by morphology effects. Calculations of κ derived from bulk chemical composition assuming

different effective densities ρ_{eff} suggest the highly non-spherical soot particle shape as the main reason for the absence of CCN activation in the beginning of the experiments. The particles' morphology also affected the H-TDMA measurements explaining hygroscopic growth factors <1 and negative values for the apparent κ. Existence of morphology changes due to the exposure of the particles to high humidity were shown with alternate operation of a pre-humidifier in front of the H-TDMA. Restructuring of aged soot under high RH was observed in the H-TDMA, suggesting the presence of non-spherical soot particle after several hours of photochemical ageing, when these particles can already take up water or interact with water. The apparent κ values for diesel soot should be considered as a lower limit as discussed in detail above.

SOA from the pure gas phase of the diesel vehicle (without any soot particles) was studied as well. We conclude that the ranges of 0.06–0.12 for $\kappa_{\text{H-TDMA}}$ and 0.09–0.14 for κ_{CCN} are representative for the pure organic fraction of photochemically aged diesel soot. These values appear to be more useful to be included in models than κ values for the entire soot (apparent κ values mentioned above) which are affected by morphology changes and are quite diameter dependent. The hygroscopicity values from pure diesel SOA formed here correspond to semi-volatile oxygenated organic aerosol found in other studies (Jimenez *et al* 2009, Duplissy *et al* 2011). The κ values are in a relatively narrow range and with known mass fractions of organics and BC one can calculate the resulting κ values of mixed particles. These values can be used to improve the description of particle hygroscopicity in global models (e.g. Liu and Wang 2010).

Mobility diameter based measurements can lead to wrong particle sizing and underestimation of the hygroscopicity for soot measurements due to morphology changes as demonstrated. A combined diameter and mass related measurement as done by other studies (e.g. Zhang *et al* 2008, Kuwata *et al* 2009) is advantageous for fractal-like particles with agglomerate structures such as soot. But it is not simply a critical mass of soluble matter that determines the hygroscopicity. H-TDMA measurements allow us to detect hygroscopic growth factors of soluble particles due to water absorption. However, they cannot be used to distinguish between hydrophobic and insoluble but hydrophilic particles, as both particle types appear at GF $\approx$ 1.0. In contrast, CCNC measurements allow us in principle to distinguish between hydrophilic and hydrophobic particles. However, the observed CCN inactivity of fresh diesel exhaust at SS corresponding to $\kappa = 0$, assuming spherical particles for the theoretical calculation, is more likely caused by non-sphericity effects during particle selection by mobility diameter rather than true hydrophobicity. Thus the term hydrophobic particles should be treated carefully.

A certain amount of organics (SOA and aged POA) on aerosols with a relatively low fractal dimension is needed to quantitatively measure mobility diameter based hygroscopicity and CCN activation. The hygroscopicity measurement of soot (BC and organics) remains challenging, especially with mobility diameter based methods, due to the fractal morphology of soot agglomerates.

Acknowledgments

The authors thank René Richter and Günther Wehrle for their great support with the construction of the H-TDMA instrument and for solving various smog chamber issues. We would like to thank Marie Laborde for her support during the measurements as well as interesting discussions on BC, and acknowledge the other people of the PSI smog chamber team. This work was supported by the IMBALANCE project of the Competence Center Environment and Sustainability of the ETH Domain (CCES), by the NEADS project of the Competence Center Energy and Mobility (CCEM), as well as the Swiss National Science Foundation. PFD is grateful for postdoctoral research support from the US-NSF (IRFP No. 0701013).

References

Baltensperger U *et al* 2002 Urban and rural aerosol characterization of summer smog events during the PIPAPO field campaign in Milan, Italy *J. Geophys. Res.* **107** 8193

Chirico R *et al* 2010 Impact of aftertreatment devices on primary emissions and secondary organic aerosol formation potential from in-use diesel vehicles: results from smog chamber experiments *Atmos. Chem. Phys.* **10** 11545–63

Chung S H and Seinfeld J H 2002 Global distribution and climate forcing of carbonaceous aerosols *J. Geophys. Res.-Atmos.* **107** 4407

Cross E S, Slowik J G, Davidovits P, Allan J D, Worsnop D R, Jayne J T, Lewis D K, Canagaratna M and Onasch T B 2007 Laboratory and ambient particle density determinations using light scattering in conjunction with aerosol mass spectrometry *Aerosol Sci. Technol.* **41** 343–59

DeCarlo P F, Slowik J G, Worsnop D R, Davidovits P and Jimenez J L 2004 Particle morphology and density characterization by combined mobility and aerodynamic diameter measurements. Part 1: theory *Aerosol Sci. Technol.* **38** 1185–205

Duplissy J *et al* 2011 Relating hygroscopicity and composition of organic aerosol particulate matter *Atmos. Chem. Phys.* **11** 1155–65

Gysel M, McFiggans G B and Coe H 2009 Inversion of tandem differential mobility analyser (TDMA) measurements *J. Aerosol Sci.* **40** 134–51

Gysel M, Nyeki S, Weingartner E, Baltensperger U, Giebl H, Hitzenberger R, Petzold A and Wilson C W 2003 Properties of jet engine combustion particles during the PartEmis experiment: hygroscopicity at subsaturated conditions *Geophys. Res. Lett.* **30** 1566

Hitzenberger R, Giebl H, Petzold A, Gysel M, Nyeki S, Weingartner E, Baltensperger U and Wilson C W 2003 Properties of jet engine combustion particles during the PartEmis experiment. Hygroscopic growth at supersaturated conditions *Geophys. Res. Lett.* **30** 1779

IPCC 2007 Summary for policy makers *Climate Change 2007: The Physical Science Basis. Contribution of Working Group I to the Fourth Assessment Report of the Intergovernmental Panel on Climate Change* ed S Solomon, D Qin, M Manning, Z Chen, M Marquis, K B Averyt, M Tignor and H L Miller (Cambridge: Cambridge University Press)

Jacobson M Z 2001 Strong radiative heating due to the mixing state of black carbon in atmospheric aerosols *Nature* **409** 695–7

Jimenez J L *et al* 2009 Evolution of organic aerosols in the atmosphere *Science* **326** 1525–9

Jurányi Z *et al* 2009 Influence of gas-to-particle partitioning on the hygroscopic and droplet activation behaviour of alpha-pinene secondary organic aerosol *Phys. Chem. Chem. Phys.* **11** 8091–7

Kim J J, Smorodinsky S, Lipsett M, Singer B C, Hodgson A T and Ostro B 2004 Traffic-related air pollution near busy roads—the East Bay children's respiratory health study *Am. J. Respir. Crit. Care Med.* **170** 520–6

Kittelson D B 1998 Engines and nanoparticles: a review *J. Aerosol Sci.* **29** 575–88

Koehler K A, DeMott P J, Kreidenweis S M, Popovicheva O B, Petters M D, Carrico C M, Kireeva E D, Khokhlova T D and Shonija N K 2009 Cloud condensation nuclei and ice nucleation activity of hydrophobic and hydrophilic soot particles *Phys. Chem. Chem. Phys.* **11** 7906–20

Koelmans A A, Jonker M T O, Cornelissen G, Bucheli T D, Van Noort P C M and Gustafsson O 2006 Black carbon: the reverse of its dark side *Chemosphere* **63** 365–77

Kuwata M, Kondo Y and Takegawa N 2009 Critical condensed mass for activation of black carbon as cloud condensation nuclei in Tokyo *J. Geophys. Res.-Atmos.* **114** D20202

Laden F, Neas L M, Dockery D W and Schwartz J 2000 Association of fine particulate matter from different sources with daily mortality in six US cities *Environ. Health Perspect.* **108** 941–7

Leskinen A P, Jokiniemi J K and Lehtinen K E J 2007 Transformation of diesel engine exhaust in an environmental chamber *Atmos. Environ.* **41** 8865–73

Lewis K A *et al* 2009 Reduction in biomass burning aerosol light absorption upon humidification: roles of inorganically-induced hygroscopicity, particle collapse, and photoacoustic heat and mass transfer *Atmos. Chem. Phys.* **9** 8949–66

Liu X H and Wang J A 2010 How important is organic aerosol hygroscopicity to aerosol indirect forcing? *Environ. Res. Lett.* **5** 044010

Lohmann U and Feichter J 2005 Global indirect aerosol effects: a review *Atmos. Chem. Phys.* **5** 715–37

Massoli P *et al* 2010 Relationship between aerosol oxidation level and hygroscopic properties of laboratory generated secondary organic aerosol (SOA) particles *Geophys. Res. Lett.* **37** L24801

Meier J, Wehner B, Massling A, Birmili W, Nowak A, Gnauk T, Bruggemann E, Herrmann H, Min H and Wiedensohler A 2009 Hygroscopic growth of urban aerosol particles in Beijing (China) during wintertime: a comparison of three experimental methods *Atmos. Chem. Phys.* **9** 6865–80

Park K, Cao F, Kittelson D B and McMurry P H 2003 Relationship between particle mass and mobility for diesel exhaust particles *Environ. Sci. Technol.* **37** 577–83

Paulsen D, Dommen J, Kalberer M, Prevot A S H, Richter R, Sax M, Steinbacher M, Weingartner E and Baltensperger U 2005 Secondary organic aerosol formation by irradiation of 1,3,5-trimethylbenzene-NO_x-H_2O in a new reaction chamber for atmospheric chemistry and physics *Environ. Sci. Technol.* **39** 2668–78

Petters M D and Kreidenweis S M 2007 A single parameter representation of hygroscopic growth and cloud condensation nucleus activity *Atmos. Chem. Phys.* **7** 1961–71

Petters M D, Wex H, Carrico C M, Hallbauer E, Massling A, McMeeking G R, Poulain L, Wu Z, Kreidenweis S M and Stratmann F 2009 Towards closing the gap between hygroscopic growth and activation for secondary organic aerosol—Part 2: theoretical approaches *Atmos. Chem. Phys.* **9** 3999–4009

Pope C A and Dockery D W 2006 Health effects of fine particulate air pollution: lines that connect *J. Air Waste Manage. Assoc.* **56** 709–42

Popovicheva O, Persiantseva N M, Shonija N K, DeMott P, Koehler K, Petters M, Kreidenweis S, Tishkova V, Demirdjian B and Suzanne J 2008a Water interaction with hydrophobic and hydrophilic soot particles *Phys. Chem. Chem. Phys.* **10** 2332–44

Popovicheva O B, Persiantseva N M, Tishkova V, Shonija N K and Zubareva N A 2008b Quantification of water uptake by soot particles *Environ. Res. Lett.* **3** 025009

Ramanathan V and Carmichael G 2008 Global and regional climate changes due to black carbon *Nature Geosci.* **1** 221–7

Robinson A L, Donahue N M, Shrivastava M K, Weitkamp E A, Sage A M, Grieshop A P, Lane T E, Pierce J R and Pandis S N 2007 Rethinking organic aerosols: semivolatile emissions and photochemical aging *Science* **315** 1259–62

Rose D *et al* 2011 Cloud condensation nuclei in polluted air and biomass burning smoke near the mega-city Guangzhou, China—Part 2: size-resolved aerosol chemical composition, diurnal cycles, and externally mixed weakly CCN-active soot particles *Atmos. Chem. Phys.* **11** 2817–36

Saathoff H, Naumann K H, Schnaiter M, Schock W, Mohler O, Schurath U, Weingartner E, Gysel M and Baltensperger U 2003 Coating of soot and $(NH_4)_2SO_4$ particles by ozonolysis products of alpha-pinene *J. Aerosol Sci.* **34** 1297–321

Stratmann F *et al* 2010 Examination of laboratory-generated coated soot particles: an overview of the LACIS experiment in november (LExNo) campaign *J. Geophys. Res.-Atmos.* **115** 12

Topping D O, McFiggans G B and Coe H 2005 A curved multi-component aerosol hygroscopicity model framework: part 1—inorganic compounds *Atmos. Chem. Phys.* **5** 1205–22

Tritscher T *et al* 2011 Volatility and hygroscopicity of aging secondary organic aerosol in a smog chamber *Atmos. Chem. Phys. Discuss.* **11** 7423–67

Wang J, Cubison M J, Aiken A C, Jimenez J L and Collins D R 2010 The importance of aerosol mixing state and size-resolved composition on CCN concentration and the variation of the importance with atmospheric aging of aerosols *Atmos. Chem. Phys.* **10** 7267–83

Weingartner E, Baltensperger U and Burtscher H 1995 Growth and structural change of combustion aerosols at high relative humidity *Environ. Sci. Technol.* **29** 2982–6

Weingartner E, Burtscher H and Baltensperger U 1997 Hygroscopic properties of carbon and diesel soot particles *Atmos. Environ.* **31** 2311–27

Xue H X, Khalizov A F, Wang L, Zheng J and Zhang R Y 2009 Effects of coating of dicarboxylic acids on the mass–mobility relationship of soot particles *Environ. Sci. Technol.* **43** 2787–92

Zelenay V *et al* 2011 Aging fingerprints in combustion particles *Atmos. Chem. Phys. Discuss.* **11** 14455–93

Zhang R Y, Khalizov A F, Pagels J, Zhang D, Xue H X and McMurry P H 2008 Variability in morphology, hygroscopicity, and optical properties of soot aerosols during atmospheric processing *Proc. Natl Acad. Sci. USA* **105** 10291–6